Scientific Contributions Oil & Gas, Vol. 46. No. 3, December: 145-159

SCIENTIFIC CONTRIBUTIONS OIL AND GAS
Testing Center for Oil and Gas
LEMIGAS

Journal Homepage:http://www.journal.lemigas.esdm.go.id
ISSN: 2089-3361, e-ISSN: 2541-0520

Relative Amplitude Preservation Analysis on Interpolation Methods of The Unaliased F-K Trace Interpolation and Regularized Nonstationary Autoregression

Wahyu Triyoso[1] and Sunawar Kunaifi[2]

[1]Department of Geophysical Engineering, Faculty of Mining and Petroleum Engineering, Institut Teknologi Bandung
Ganesha 10 Street, Bandung 40132, Indonesia

[2]Halliburton
Taman Tekno Industrial & Warehousing Area, Blok D No. 1, South Tangerang City, 15314, Banten, Indonesia

Corresponding author: wtriyoso@gmail.com.

Manuscript received: October 23st, 2023; Revised: November 15st, 2023
Approved: December 14st, 2023; Available online: December 23st, 2023

ABSTRACT - The seismic data interpolation method has been widely used to increase the fold coverage in seismic data processing. This technique could be applied to convert multi-2D lines into pseudo-3D, which is an alternative to obtaining 3D seismic volume data due to the relatively high acquisition cost. However, the quality of the seismic interpolation results is not the same as the real 3D seismic data acquisition results. This study concientiourly analyzed these differences to understand how accurate the results were. There are two methods used for data interpolation, especially Unaliased f-k trace interpolation (UFKI) and Regularized Interpolation Nonstationary Autoregression (RNA) methods, which are applied to 2D pre-stack data to increase the fold coverage and 3D data to convert multi-2D lines into pseudo-3D. Then, the interpolation results on the pre-stack data are evaluated on the 2D and 3D data, and an amplitude change is analyzed. It is done to test whether the amplitude of the seismic data from the interpolation results is still relatively preserved based on the evaluation results of the changes in the AVO response. The results show that the interpolation process in the receiver and shot gather domain (UFKI and RNA) could increase the fold coverage and maintain the relative amplitude preservation and AVO response.

Keywords: seismic interpolation, ufki, rna, pseudo-3d, avo response.

How to cite this article:

Wahyu Triyoso and Sunawar Kunaifi, 2023, Relative Amplitude Preservation Analysis on Interpolation Methods of The Unaliased F-K Trace Interpolation and Regularized Nonstationary Autoregression, Scientific Contributions Oil and Gas, 46 (3) pp. 145-159. DOI.org/10.29017/SCOG.46.3.1589.

INTRODUCTION

Seismic data interpolation has been widely used and applied in seismic data processing for various purposes. The quantity of seismic data sampling significantly affects the quality, especially with respect to the frequency content. For example, consider seismic data with a four-millisecond temporal sampling. This would result in a Nyquist frequency of up to 125 Hertz. Increasing the temporal sampling to two milliseconds or one millisecond will increase the frequency of the seismic data. Spatial sampling is as important as temporal sampling; if temporal sampling is associated with vertical resolution, then spatial sampling is associated with

lateral resolution. Improving the temporal resolution of seismic data is easy and cheap, but increasing the lateral resolution is very expensive because it requires more seismic acquisition equipment, time, and human resources (Liu and Fomel, 2011); (Lan et al., 2022); (Triyoso et al., 2023). Seismic data with sparse spatial sampling will result in poor quality seismic data processing results. For example, when the Radon transform algorithm is used in applications, it fails if the common depth point spacing is too large. Under these conditions, spatial aliasing occurs, which prevents the algorithm from successfully demultiplying (Foster and Mosher, 1992); (Zhang et al., 2019).

The interpolation method could be applied to sparse spatial sampling data to obtain a denser spatial sampling. The smaller spatial sampling of the data improves the quality of the seismic processing results. The interpolation method can be applied to sparse spatial sampling data to obtain a denser spatial sampling. The denser spatial sampling will improve the quality of the seismic processing results. Figure 1 shows the results of seismic migration on seismic data with sparse to dense spatial sampling (Spitz, 1991).

The results show that denser spatial sampling produces a more reliable subsurface structure model.(Trad, 2009) and others (Carozzi and Sacchi, 2019); (Zhang et al., 2019); (Bayati and Trad, 2023) interpolated the 3D seismic data to increase the fold coverage, and then compared the data processing results of data with and without interpolation. Figure 2 shows the result of data processing with interpolation, which shows an increase in quality compared to without interpolation. The data processing results become more reliable as the interpolation increases the fold coverage of the data. Various interpolation methods have been developed and widely used in seismic data processing. Some methods are applied in the frequency domain and some in the time domain. (Gülünay and Chambers, 1996) and others (Xie et al., 2020); (Cao et al., 2020) introduce the unaliased f-k trace interpolation (UFKI) method in the frequency domain, which has been used for a long time. (Fomel, 2009) and others (Liu and Fomel, 2011); (Liu and Chen, 2018); (Liu et al., 2019) introduce the Regularized Nonstationary Autoregression (RNA) interpolation method in the time domain. (Triyoso et al., 2020) and (Muhtar et al., 2021) showed the application of the Common Reflection Surface (CRS) as an alternative method for seismic interpolation in the time domain.

It is important to better understand the advantages and disadvantages of time and frequency domain interpolation applications. This knowledge allows for optimal decision making when applying these techniques. The f-k interpolation method uses the low-frequency non-alias portion of the data to interpolate the high-frequency alias. Therefore, it can properly handle the spatial domain.

The application of seismic data interpolation that has also been widely used is interpolation to convert multi-2D line data into 3D seismic data volume. It is called pseudo-3D. The pseudo-3D seismic acquisition is a seismic acquisition with 2D geometry where the distance between the lines is dense, namely 50m to 200m. The main reason for performing pseudo-3D seismic acquisition is cost, which is much cheaper than true 3D seismic acquisition.

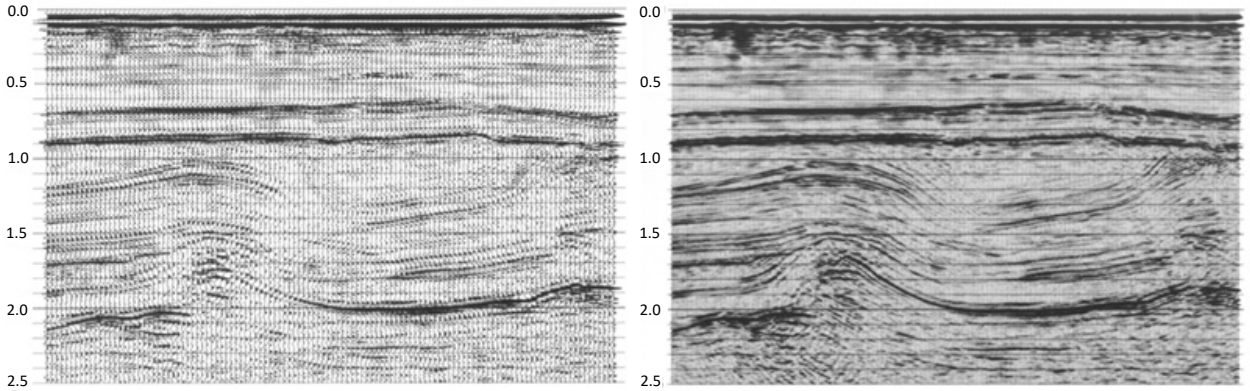

Figure 1
Result of seismic migration of 75m (left) and 25m (right) spatial sampling (Spitz, 1991). It shows that denser spatial sampling produces a more reliable subsurface structure model.

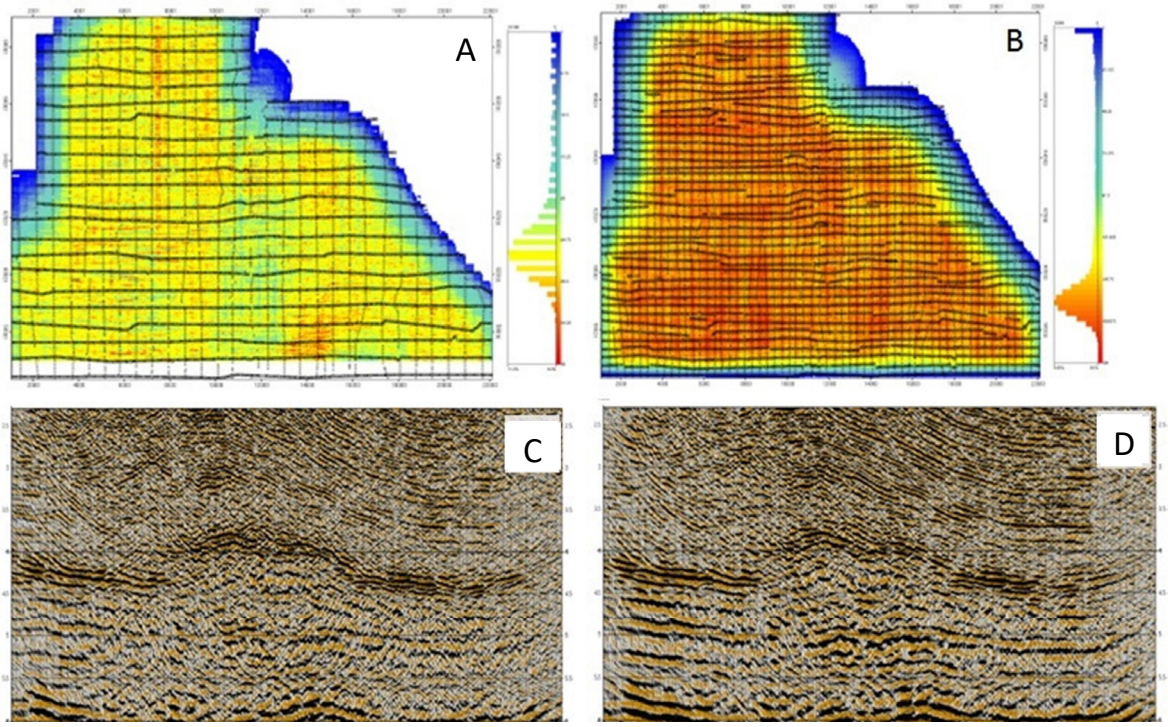

Figure 2
Fold coverage before (A) and after (B) interpolation; stack data before (C) and after (D) interpolation (Trad, 2009).

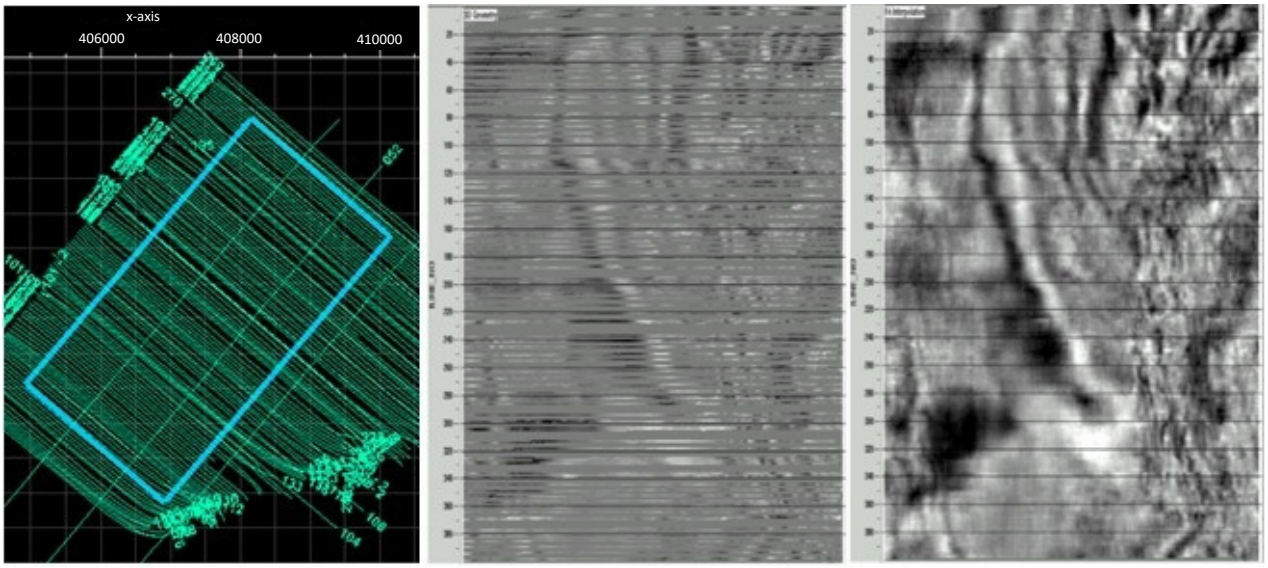

Figure 3
The 2D multiline (left), 2D multiline time slice (middle), and pseudo-3D time slice (right) (Riandy 2014).

For example, (Riandy, 2014) interpolated seismic data from 2D seismic multiline data with an intertrack distance of about 50m to a 3D seismic volume with an inline to xline distance of 12.5m. This seismic data interpolation is performed on post-stack data prior to migration to 3D post-stack data, then 3D post-stack migration is performed. The conversion of multi-2D line data into 3D seismic volumes showed excellent results in increasing lateral resolution. This can be seen in Figure 3 below.

The most important thing to note about the seismic interpolation results is to evaluate whether the result still retains the preserved amplitude. In other words, it is essential to see whether the seismic data that has undergone the interpolation process is still feasible for advanced processing and

further work in reservoir characterization, such as AVO analysis for hydrocarbon detection, seismic inversion, or multi-attribute analysis.

The motivation of this study is to compare the unaliased f-k trace interpolation (UFKI) and regularized nonstationary autoregression (RNA) interpolation methods in relative amplitude preservation. Therefore, the AVO response of 2D and 3D seismic as the interpolation results are discussed in this study. The interpolation of 2D seismic data focuses on pre-stack interpolation to increase the fold coverage. In contrast, the interpolation of 3D seismic data will focus on multi-2D line conversion into pseudo-3D seismic data of the partial stack of near and far offsets.

METHODOLOGY

The UFKI method was proposed by (Gülünay and Chambers, 1996, 1997) and others (Xie et al., 2020); (Cao et al., 2020) - the frequency domain technique that has long been used in seismic data processing. (Fomel, 2007, 2009) and others (Liu and Fomel, 2011); (Liu and Chen, 2018); (Liu et al., 2019) introduced the RNA interpolation method in the time domain. Thus, understanding the basic theory of these two methods would make it easier to compare the advantages and disadvantages of these two methods.

Data

Two types of data are used in this study: synthetic 2D and 3D seismic data. In the case of 2D seismic data, the analysis was performed using synthetic data from the Marmousi-2 model (Martin et al., 2006), which consists of volume Vp, Vs, and density. Preserved amplitude analysis was performed using AVO analysis on the Water Wet Sand, Oil Sand, and Gas Sand zones so that the effect of amplitude changes due to the interpolation process can be known with certainty. In the case of 3D seismic data, the analysis was performed using offshore seismic data from the Penobscot area, Sable Islands, Canada. The data have been processed by prestack time migration (PSTM). The objective is to evaluate the effect of interpolation on the reservoir distribution from the seismic attributes of P and S impedance.

Unaliased f-k Trace Interpolation (UFKI)

The algorithm of unaliased f-k domain trace interpolation (Gülünay and Chambers, 1996, 1997); (Xie et al., 2020); (Cao et al., 2020) can be shown as follows (Figure 4).

Regularized nonstationary autoregression (rna) interpolation method

(Liu and Fomel, 2011) and others (Liu and Chen ,2018); (Yang et al., 2020) have made significant contributions to the development of interpolation techniques for aliased seismic data. Their approach, which includes adaptive prediction error filtering and regularized nonstationary autoregression, has shown promising results in effectively interpolating aliased seismic data. As a result, these methods have improved the ability to interpret and analyze subsurface structures in seismic data. Instead of cutting the data into overlapping windows (patching), a popular method for dealing with nonstationarity, they obtain smooth nonstationary PEF coefficients by solving a global regularized least-squares problem. They used the two-step strategy similar to that of (Claerbout, 1992) and others (Crawley, 1998, 1999); (Yang et al., 2020). However, they computed the adaptive prediction error filter (PEF) using regularized nonstationary autoregression (Fomel, 2009); (Liu and Fomel, 2011); (Liu and Chen, 2018) to deal with nonstationarity and aliasing. The key idea is shape regularization (Fomel, 2007); (Liu and Fomel, 2011); (Liu and Chen, 2018) to constrain the spatial smoothness of the filter coefficients. (Fomel, 2007, 2009) and others (Liu and Fomel, 2011); (Liu and Chen, 2018); (Liu et al., 2019) define a stationary data regression formulation as follows,

$$e(\mathbf{x}) = m(\mathbf{x}) - \sum_{k=1}^{N} a_k s_k(\mathbf{x}) \tag{1}$$

Where, e(x): error, m(x): master signal, S(x): slave signal, a_k: regression coefficient and x: space

The RNA interpolation has two steps, such as the PEF estimation and the second step of applying the PEF to estimate the data interpolation (Liu and Fomel 2011); (Liu and Chen 2018); (Liu et al. 2019). PEF estimation can be written as follows,

$$\begin{aligned}\widetilde{B_n}(t,x) \;=\; & \arg\min_{B_n} \|S(t,x) - \sum_{n=1}^{N} B_n(t,x) S(t-i,x-j)\|_2^2 \\ & + \varepsilon^2 \sum_{n=1}^{N} \|\mathbf{D}[B_n(t,x)]\|_2^2 ,\end{aligned} \tag{2}$$

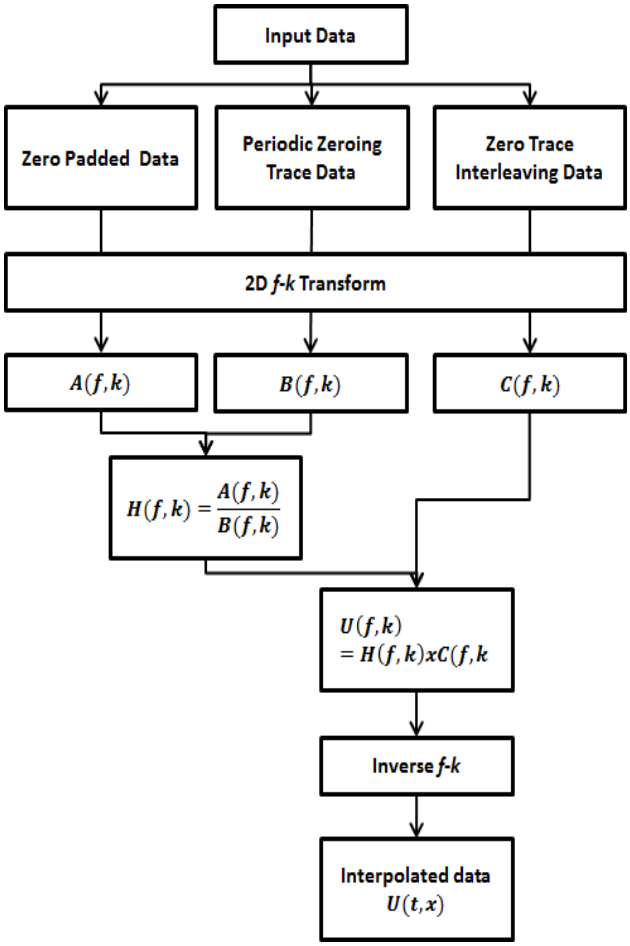

Figure 4
The UFKI interpolation flowchart (Gülünay and Chambers, 1996, 1997).

where $S_n(t,x) = S(t - m_i\Delta t, x - m_{j\Delta t})$, representing the causal translation of S(t,x), with the temporal shift index i and the spatial shift index j scaled by the decimation interval m. Note that the predefined constant m uses the interlace value as the interval; i.e., the shift interval is equal to 2. The subscript n is the general shift index for both time and space. The total number of i and j is N. D is the regularization operator, and ε is a scalar regularization parameter. All coefficients Bn(t,x) are estimated simultaneously in a time-space variant manner. This approach has been described by (Fomel, 2007) and others (Liu and Fomel, 2011); (Liu and Chen, 2018); (Liu et al., 2019) as regularized non-stationary autoregression (RNA)..

In the second step, the Bn prediction coefficient is used to estimate the empty trace on incomplete aliased data S(t,x). The formulation of the data interpolation estimates is as follows,

$$\widetilde{S}(t,x) = \arg\min_{S} \|S(t,x) - \sum_{n=1}^{N} \widetilde{B}_n(t,x) S(t-i', x-j')\|_2^2 \quad (3)$$

Where B_n is the prediction coefficient obtained from the PEF estimation, $\hat{S}(t,x)$ is the interpolated data, $S(t,x)$ is incompletely aliased data, i.e., the known input data (S_k) inserts an empty trace between each trace (S_z), $S(t\text{-}i',x\text{-}j')$ is the translation of $S(t,x)$ in time and space.

RESULT AND DISCUSSION

2D Seismic data

The synthetic data obtained from forward modeling is divided into three datasets. The first dataset contains the initial forward modeling results. The second dataset expands upon seismic interpolation

by applying trace decimation with a ratio of 4:1 using the UFKI method, as shown in Figure 5. The final dataset is created by interpolating data using the RNA method. All three datasets are processed with identical parameters and flow for comparative purposes. RMS velocity analysis is conducted exclusively on the original dataset. The results are then applied to the UFKI and RNA interpolated datasets. This strategy ensures that amplitude alterations in the interpolated data stem exclusively from the interpolation process, not parameter or velocity discrepancies. This section explains the procedure for processing 2D synthetic data from forward modeling. The processed results are then compared directly with the original data and outputs from UFKI interpolation and RNA to evaluate the strengths and weaknesses of each method.

Data Decimation

In forward modeling, the data is reduced by a 4:1 ratio based on the direction of both the shot point and the receiver. The geophones were initially spaced 12.5 m apart, but this is expanded to 50 m in the processed data. Similarly, the distance between original shot points, initially set at 25 m, is extended to 100 m. This transformation is shown in the table below.

The data that has been reduced by decimation is then reorganized with new headers to create a CMP gather, as illustrated in Figure 5. Panel (a) shows the CMP gather before decimation, while panel (b) shows it after decimation.

Data Interpolation

The decimated data is interpolated in the direction of both the shot point and receiver at a ratio of 1:4. This ensures that the distance between the geophone and the shot point reverts to that of the original data. The interpolation process involves two stages: first in the geophone direction, then in the direction of the shot point. Figure 6 illustrates the outcome of interpolation in the receiver direction. Figure (a) shows the original data, (b) displays the results after UFKI interpolation, and (c) features the results following RNA interpolation.

Table1
Geometry data before and after decimation

	Original Data	After Space Given
Receiver amount	240	60
Receiver Space	12,5 m	50 m
Shotpoint Space	25 m	100 m

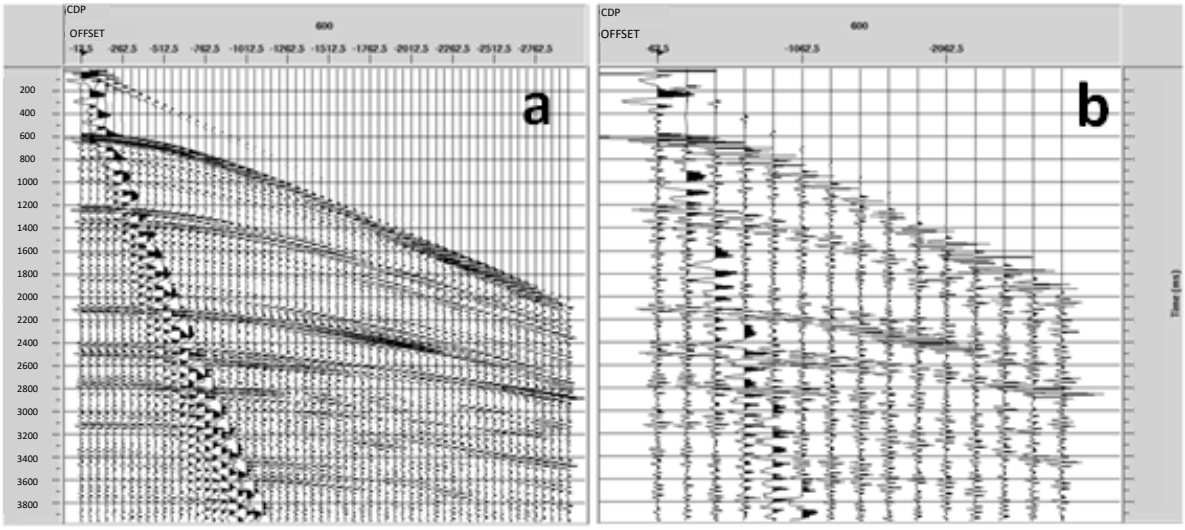

Figure 5
CMP gather before decimation (a) and after decimation (b).

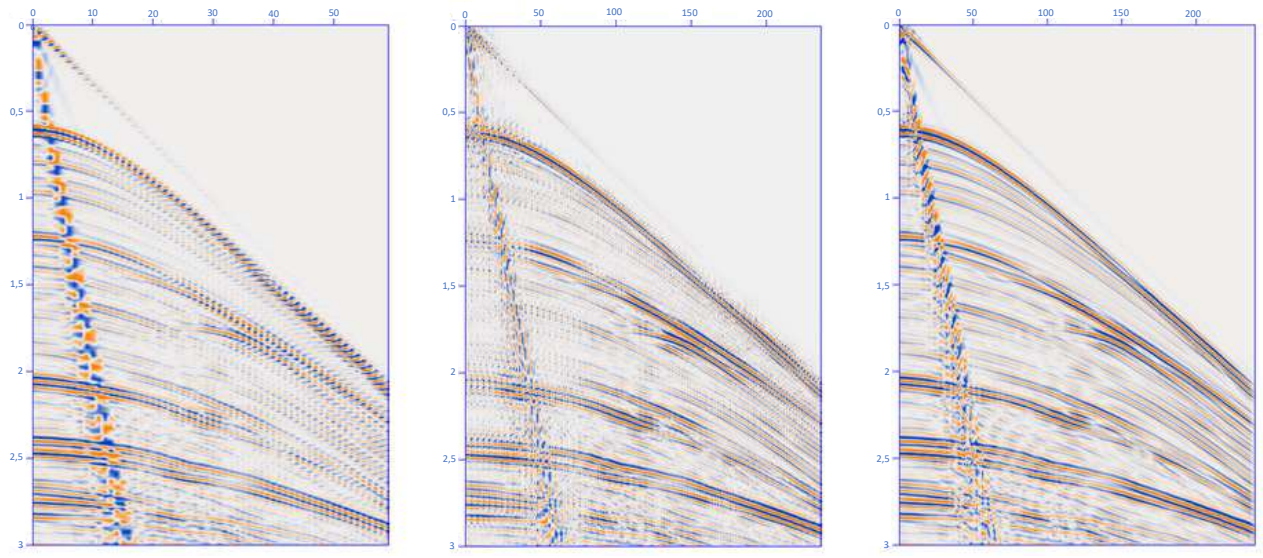

Figure 6
The results of the interpolation based on the receiver direction can be observed in three stages: (a) illustrating the original data, (b) post-UFKI interpolation, and (c) following RNA interpolation.

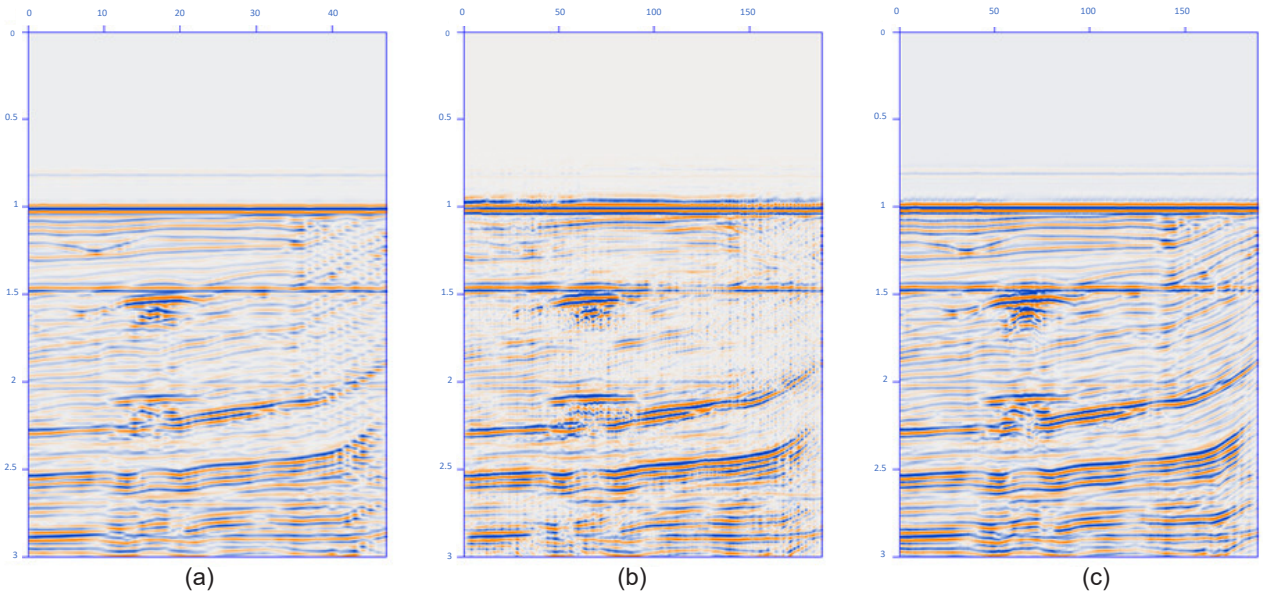

Figure 7
The results of the interpolation based on the direction of the shot point can be observed in three stages: (a) illustrating the original data, (b) post-UFKI interpolation, and (c) following RNA interpolation.

2D Interpolation analysis

The document presents an analysis of the effect of Interpolation on the Amplitude Versus Offset (AVO) response on synthetic data from the Marmousi2 reservoir (Martin et al., 2006). The study covers three distinct reservoir zones: gas reservoirs (A), oil reservoirs (B), and water reservoirs (C), which are detailed in Figure 8. The specifics of the AVO analysis vary according to the reservoirs. AVO analysis was conducted on CDP 532 for gas reservoirs, CDP 789 for oil reservoirs, and CDP 406 for water reservoirs.

The AVO analysis for the gas zone was conducted at CDP 532. The original data for this gas zone shows an intercept value (A) of -3.46 and a gradient value (B) of -13.72. The interpolated data from UFKI shows an intercept value (A) of -3.44 and a gradient value (B) of -19.21.

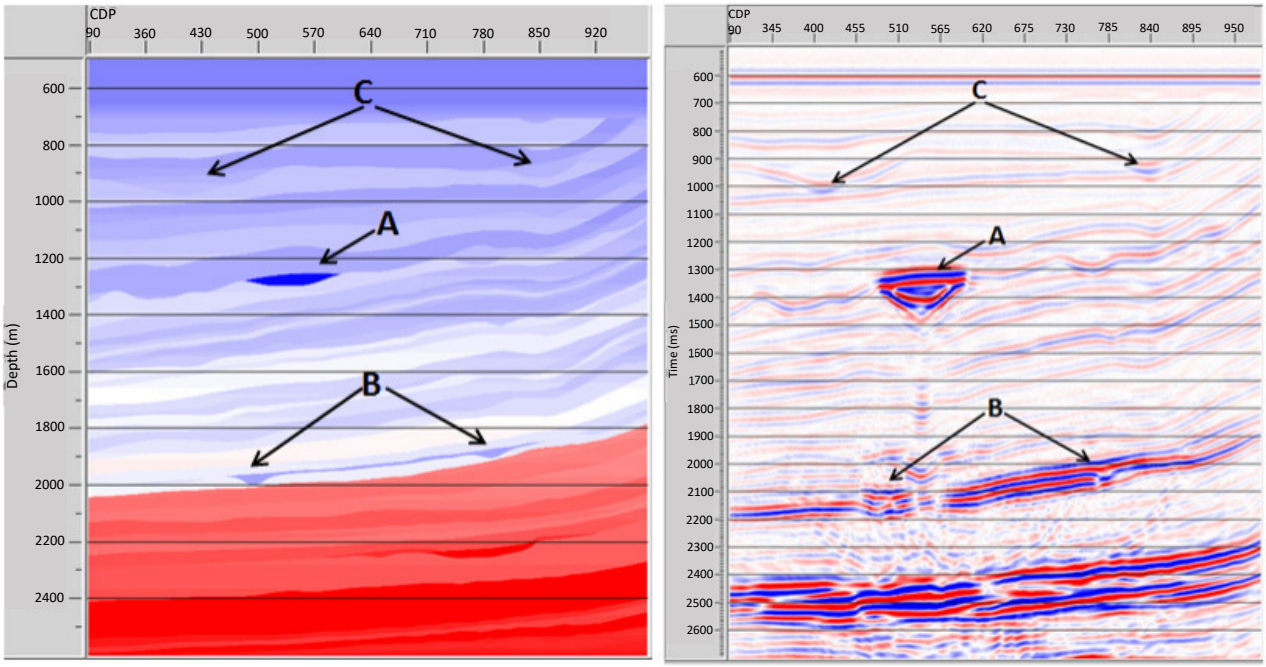

Figure 8
The Marmousi2 velocity (Vp) model (left) and PSTM stack data processing results (right), (A) gas, (B) oil,

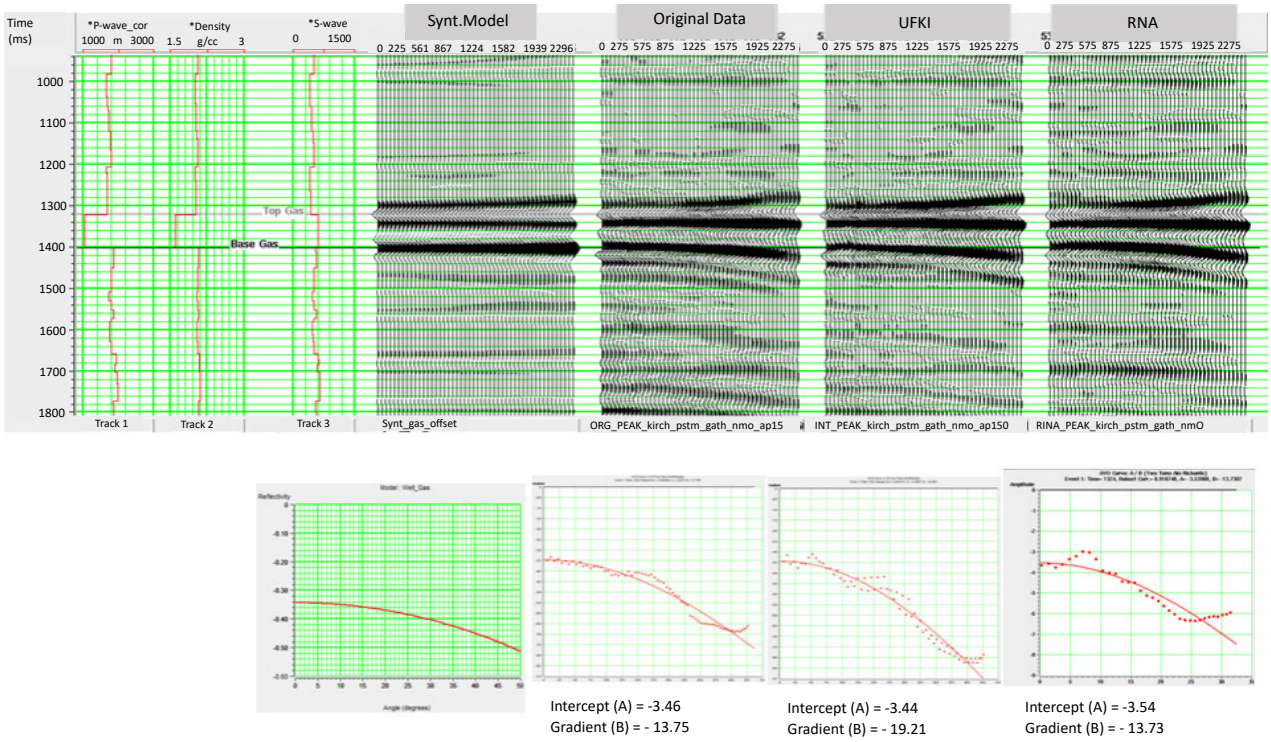

Figure 9
The AVO response of the gas zone.

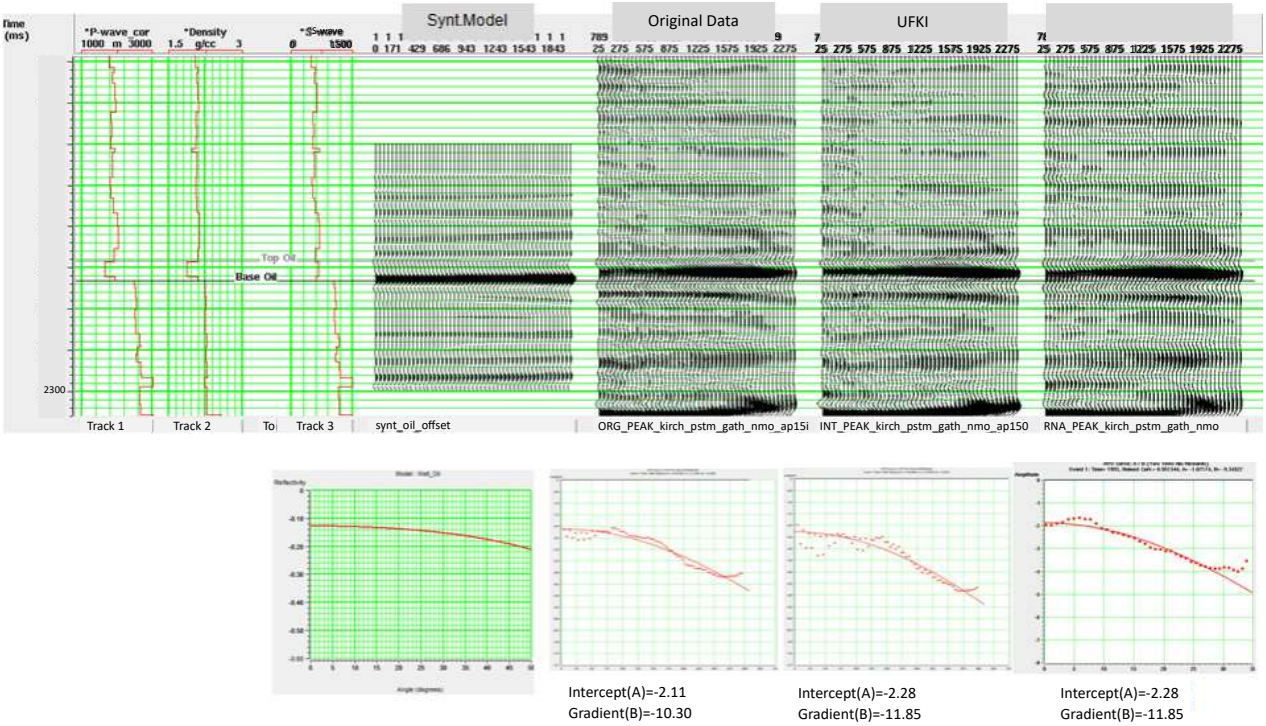

Figure 10
The AVO Response of the oil zone

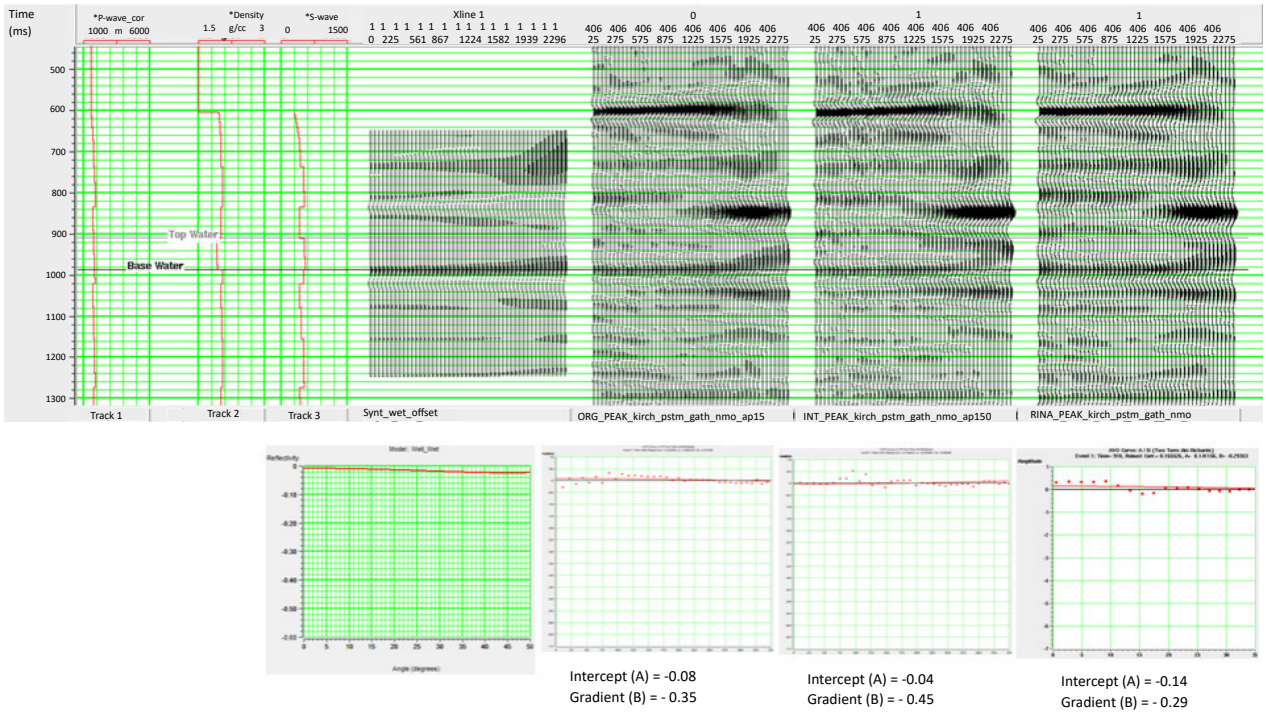

Figure 11
The AVO Response of the water zone

The data from RNA interpolation shows an intercept value (A) of -3.54 and a gradient value (B) of -13.73. The amplitude value changes after the interpolation process. This is evident from the curve in Figure 9, which shows that the amplitude value points differ between the original and interpolated data. The amplitude of the UFKI interpolation results appears more spread out, while the RNA interpolation results appear smoother. Although the amplitude's absolute value has changed, the intercept and gradient values of the interpolated data have not changed significantly. The intercept values have only changed by 0.6% for UFKI and 1.7% for RNA compared to the original data. The UFKI interpolation resulted in a 40% change in the gradient value, while the RNA changed by only 0.1%.

AVO analysis was performed on CDP 789 in the oil zone. Figure 10 displays the original data from the oil zone with an intercept value (A) of -2.11 and a gradient value (B) of -10.30. The UFKI interpolated data has an intercept value (A) of -2.28 and a gradient value (B) of -11.85. The RNA interpolation data has an intercept value (A) of -1.87 and a gradient value (B) of -9.34. The intercept value for the UFKI interpolation results changed by 8%, while the RNA interpolation results changed by 11%. It is worth noting that the gradient value resulting from the UFKI interpolation changed by 15%, while that of RNA changed by 9%.

The water reservoir does not exhibit a significant impedance contrast, and the amplitude with respect to offset remains relatively constant. Thus, the intercept and gradient values are close to zero, as depicted in Figure 11.

3D Seismic Data

Interpolation of 3D seismic data aims to determine how the process affects the reservoir distribution map. This analysis utilizes the P impedance and S seismic attributes obtained from the partial near and far stack angles using the Fatti algorithm (Fatti et al., 1994); (Huang et al., 2020); (Nie et al., 2021). The reservoir being analyzed is the spread of the sand#5 reservoir from the Missisauga Formation, as depicted in Figure 12.

The impedance of reservoir sand #5, as shown in the original data, indicates excellent distribution and thickness. Mapping of the sand#5 reservoir was performed by slicing at 2125ms in well L-30 using horizon D, as illustrated by the arrow in Figure 13. The errors resulting from the UFKI and RNA interpolation processes were evaluated by comparing the interpolated map to the original data map. The error value can be calculated using the following formula:

$$Error = \frac{(\text{Interpolated} - \text{Original})}{\text{Original}} \times 100\% \qquad (4)$$

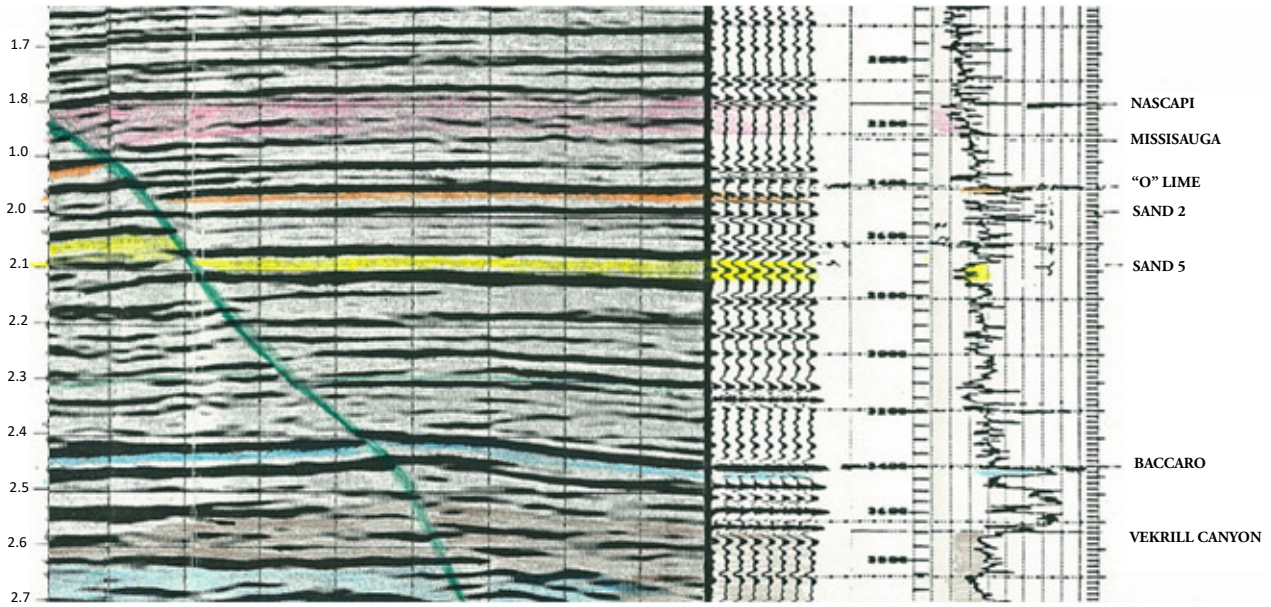

Figure 12
The correlation of sonic log and synthetic seismogram of well L-30 to seismic tie (Clack and Crane, 1997)

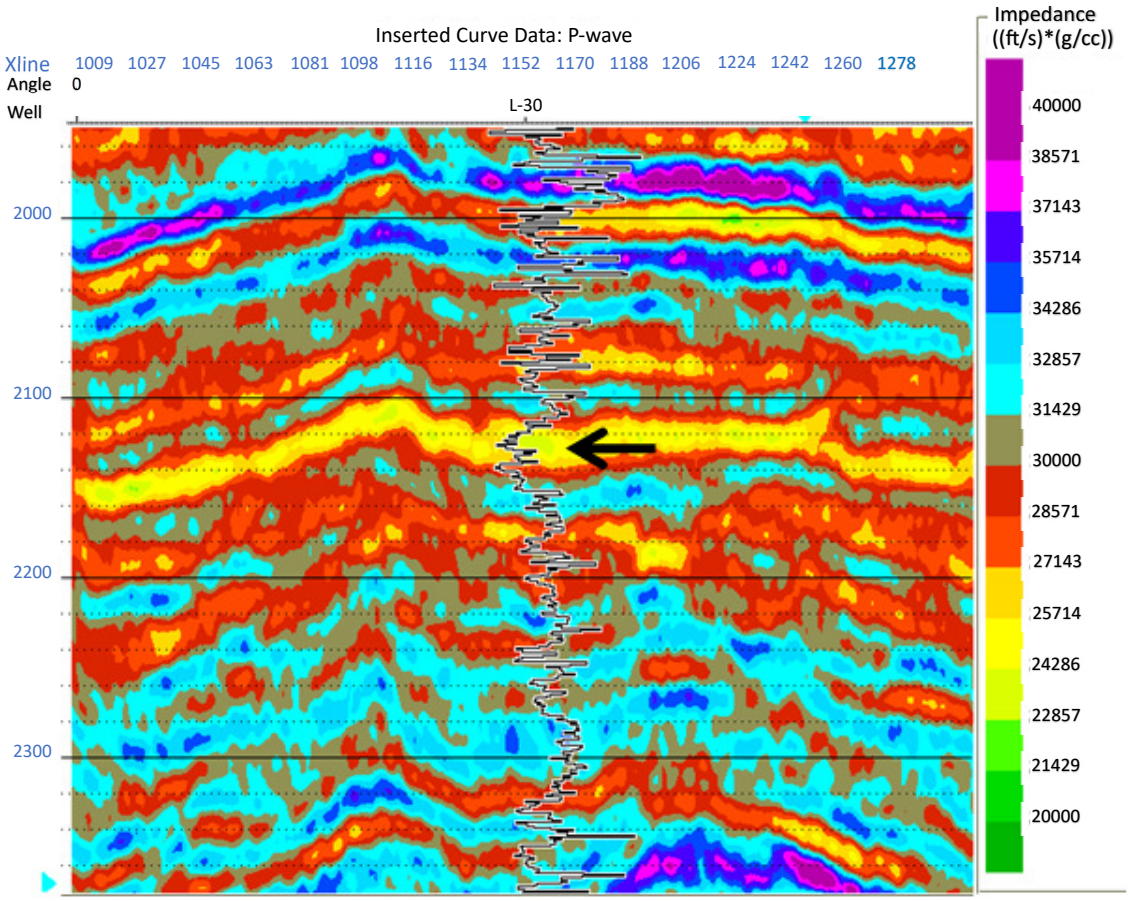

Figure 13
The P impedance section. The arrow indicates the location of the slice mapping reservoir sand #5

UFKI Interpolation

The distribution map of reservoir sand #5, resulting from the UFKI interpolation of P impedance, closely resembles the original data with a relatively small error. The error map indicates that the change in the P impedance distribution map caused by the UFKI interpolation is minimal, with a maximum of only 2-5%, as shown in Figure 14. The change in the S impedance distribution map is slightly more significant than that of the P impedance, up to 7%, as shown in Figure 15c.

RNA Interpolation

The distribution map of P impedance from reservoir sand #5, interpolated by the RNA method, closely resembles the original data with no significant changes. This is evident from the map error, which is only around 2-3%, as shown in Figure 16. However, impedance S shows slightly different results, with a more significant error map of up to 10%, as shown in Figure 17.

Both the UFKI and RNA interpolation methods resulted in minor changes to the P impedance distribution map, with the reservoir distribution remaining in the same location and only a small error of approximately 2-5%. The scattering of the S impedance resulting from UFKI and RNA interpolation had a higher error than the P impedance, but the reservoir scattering distribution did not differ significantly from the original data. The S impedance distribution map error resulting from RNA interpolation is greater than that of the UFKI method.

The study compared the RNA interpolation method and the UFKI method and found that the RNA interpolation method was slower due to its operation in the time domain and the need for iteration to estimate the PEF prediction coefficient and interpolations. However, RNA interpolation better interpolated slanted structures than UFKI despite producing smoother results. Both UFKI and RNA changed data amplitude values in the prestack interpolation process to increase fold coverage, but

there was minimal alteration to the AVO response. The 3D seismic volume data was generated using an interpolation process based on the Multi 2D line (Pseudo-3D), resulting in slightly altered P and S impedance values. However, the distribution maps remained unchanged, with an error margin below 10%. Notably, there were more significant errors in S impedance due to changes in the AVO gradients.

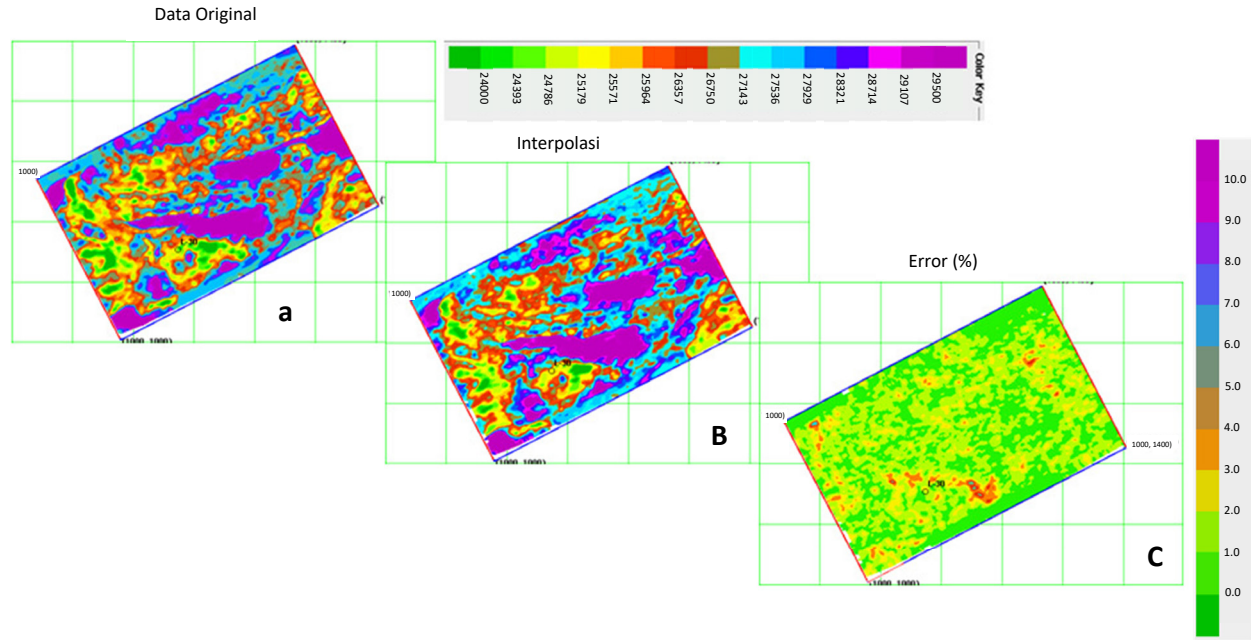

Figure 14
The P Impedance map from UFKI interpolation results, (a) original data, (b) UFKI interpolation, (c) error

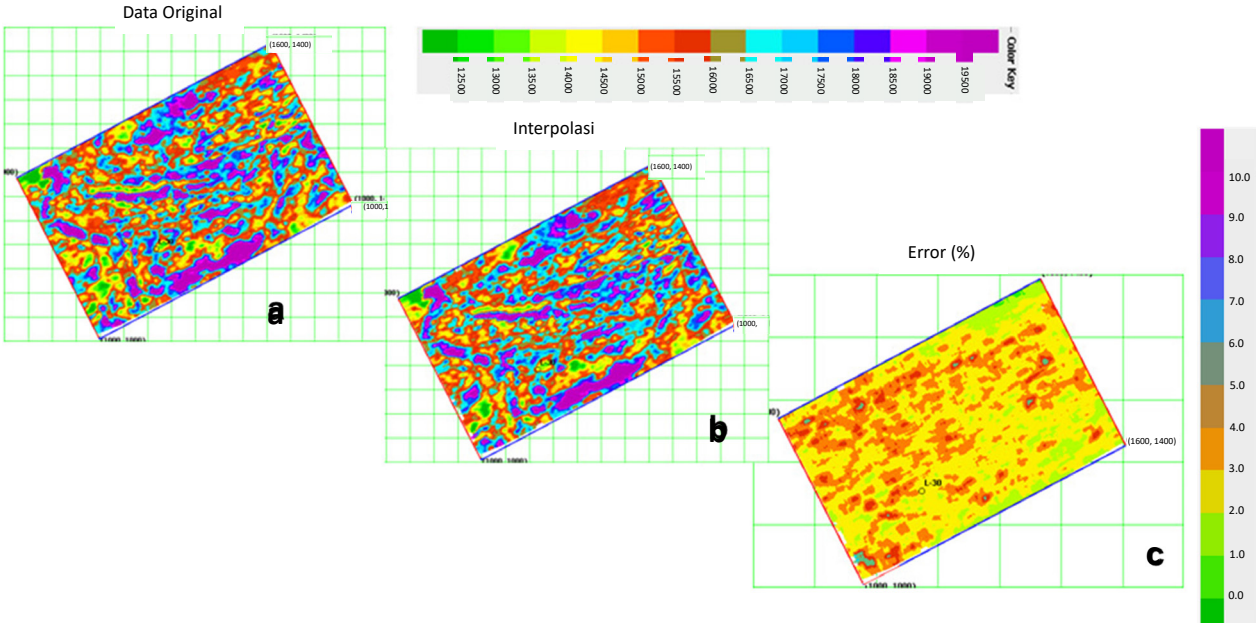

Figure 15
The S impedance map from UFKI interpolation results, (a) original data, (b) UFKI interpolation, (c) error

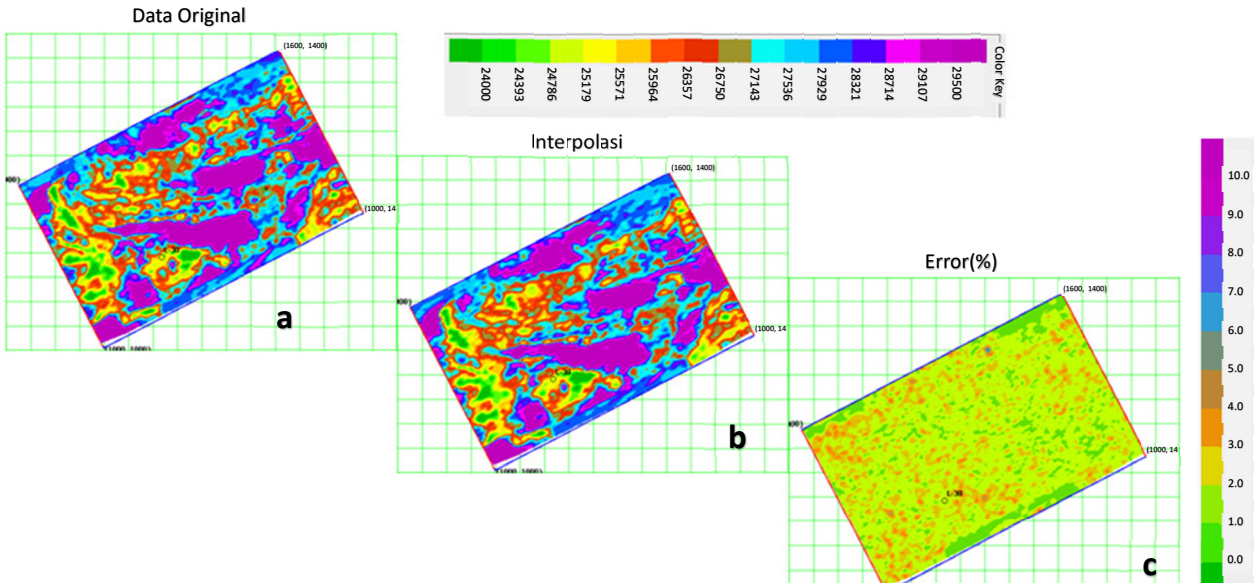

Figure 16
The P impedance map from RNA interpolation results, (a) original data, (b) UFKI interpolation, (c) error

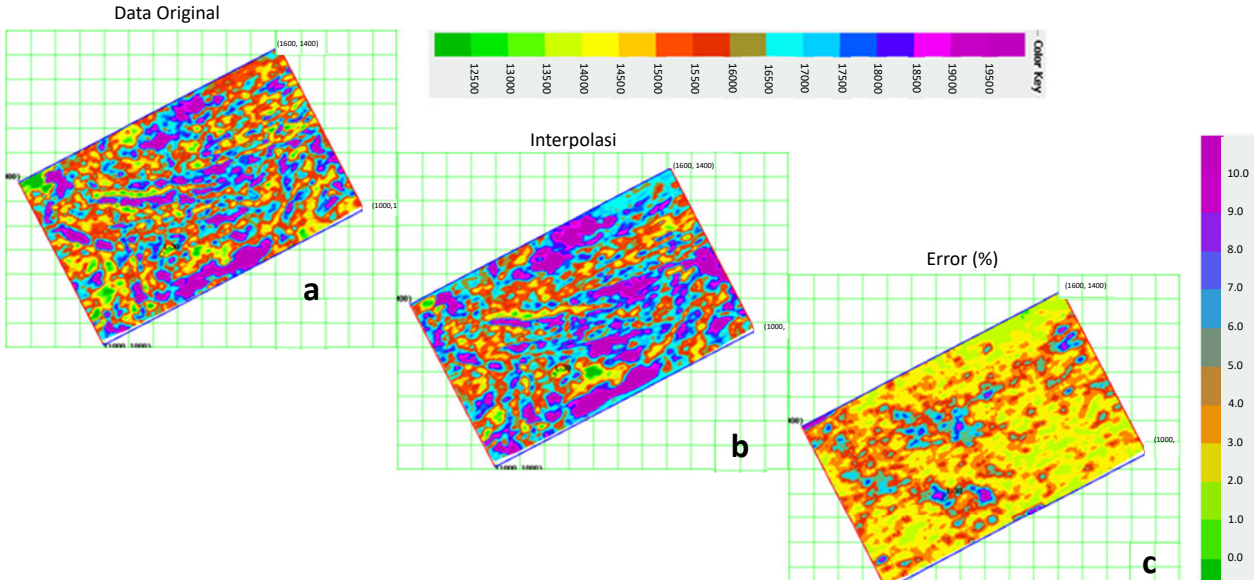

Figure 17
The s impedance map from RNA interpolation results, (a) original data, (b) UFKI interpolation, (c) error

CONCLUSION

Based on the results of this study, it can be concluded that the RNA interpolation method requires a longer processing time than the UFKI method due to its operation in the time domain and the need for iteration to estimate the PEF prediction coefficient and iterations in the interpolation process. Additionally, the UFKI interpolation method produces more random noise than the RNA interpolation method. The RNA interpolation method is better suited for interpolating slanted structures compared to the UFKI interpolation method. However, the results of the RNA method

are smoother than both the UFKI and original data. The prestack interpolation process in the receiver and shot gather domains (UFKI and RNA) increases the fold coverage but also changes the amplitude values of the data. Despite this, the AVO response (intercept and gradient) remains relatively unchanged. The Multi 2D line interpolation process into pseudo-3D alters P and S impedance values but does not affect the distribution map of P and S impedance with an error below 10%. Due to the interpolation process, the S impedance error is larger than the P impedance because the AVO gradient also changes.

The suggestions presented require further testing and evaluation for future research. The first suggestion is to convert the multi-2D line to pseudo 3D. It is important to note that the error of the interpolation result is highly dependent on the complexity of the subsurface. Therefore, further research is necessary to evaluate the distance between 2D lines used as input to obtain the optimal and reliable result. Secondly, in the case of prestack interpolation, NMO corrections must be applied before interpolation to reduce aliasing caused by data skew. Thirdly, when converting a multi-2D line to pseudo-3D interpolation, it is necessary to compare the 2D interpolation algorithms (in-line or x-line directions only) with the 3D interpolation algorithms (simultaneous in-line and x-line directions).

ACKNOWLEDGEMENT

We would like to express our gratitude for the Marmousi-2 model provided by **Martin et al. (2006)** and the offshore seismic data from the Penobscot area, Sable Islands, Canada, which were made available to us free of charge.

GLOSSARY OF TERMS

Symbol	Definition
UFKI	Unaliased f-k Interpolation
RNA	Regularized NonstationaryAutoregression
PEF	Prediction Error Filter
PSTM	Pre-stack Time Migration
NMO	Normal Move Out
AVO	Amplitude Versus Offset
CDP	Common Depth Pointc

REFERENCES

Bayati, F. and Trad, D., (2023), 3-D Data Interpolation and Denoising by an Adaptive Weighting Rank-Reduction Method Using Multichannel Singular Spectrum Analysis Algorithm. Sensors, 23, 577.

Cao, J., Cai, Z., and Liang, W., (2020), A novel thresholding method for simultaneous seismic data reconstruction and denoising. Journal of Applied Geophysics 177.

Carozzi, F. and Sacchi, M.D., (2019), Robust tensor-completion algorithm for 5D seismic data reconstruction, Geophysics, 84, V97–V109**.**

Clack, W.J.F., and Crane, J.D.T., (1997), Penobscot Prospect: Geological Evaluation And Oil Reserve Estimates: Nova Scotia Resources.

Claerbout, J. F., (1992), Earth soundings analysis: Processing versus inversion: Blackwell Scientific Publications.

Crawley, S., (1998), Shot interpolation for radon multiple suppression: 68th Annual Internat. Mtg., Soc. Expl. Geophys., Expanded Abstracts, 1238–1241.

Crawley, S., (1999), Interpolation with smoothly nonstationary prediction-error filters, Stanford Expl. Proj., Report 100, April 20, 1999, pages 181–196.

Fatti, J.L., Smith, G.C., Vail, P.J., Peter J. Strauss, P.J., Levitt, P.R., (1994), Detection of gas in sandstone reservoirs using AVO analysis: A 3-D seismic case history using the Geostack technique. GEOPHYSICS 59: 1362-1376.

Fomel, S., (2007), Shaping regularization in geophysical-estimation problems: Geophysics, 72, no. 2, R29–R36, doi: 10.1190/1.2433716.

Fomel, S., (2009), Adaptive multiple subtraction using regularized nonstationary regression: Geophysics, 74, no. 1, V25–V33, doi: 10.1190/1.3043447.

Foster, D. J., and Mosher, C. C., (1992), Suppression of multiple reflections using the Radon transform: Geophysics, 57, 386-395.

Gülünay, N., and Chambers, R. E., (1996), Unaliased f-k Domain Trace Interpolation (UFKI): 66th Ann. Internat. Mtg., Society of

Exploration Geophysicists, Expanded Abstracts, 1461–1464.

Gülünay, N., and Chambers, R. E., (1997), Generalized f-k Domain Trace Interpolation: 67th Ann. Internat. Mtg., Society of Exploration Geophysicists, Expanded Abstracts, 1100–1103.

Huang, G., Chen, X., Chen, Y., (2020), Pre-stack seismic inversion based on $L_{1-2\text{-norm}}$ regularized logarithmic absolute misfit function, Geophysical Prospecting, 2020, 68, 2419-2443.

Lan, N.Y., Zhang, F.C., Yin, X.Y., (2022), Seismic data reconstruction based on low dimensional manifold model, Petroleum Science, 19 (2022), 518-533.

Liu, Y., & Fomel, S., (2011), Seismic data interpolation beyond aliasing using regularized nonstationary autoregression. Geophysics, 76, V69-V77.

Liu, G., & Chen, X., (2018), Seismic data interpolation using frequency-domain complex nonstationary autoregression. *Geophysical Prospecting*, *66*(3), 478-497.

Liu, G., Li, C., Guo, Z., and Rao, Y., **2019**, Irregularly Sampled Seismic Data Reconstruction Using Multiscale Multidirectional Adaptive Prediction-Error Filter. IEEE Transactions on Geoscience and Remote Sensing, 57, 2909-2919.

Martin, G., Gary S.; Wiley, R., Marfurt, K.J., (2006), Marmousi2: An elastic upgrade for Marmousi. The Leading Edge. 25 (2): 156–166.

Muhtar, L.K., Triyoso, W., Fatkhan, (2021), Application of common reflection surface (CRS) to velocity variation with azimuth (VVA_z) inversion of the relatively narrow azimuth 3D seismic land data. Open Physics 2021; 19: 439–446.

Nie, W., Xiang, F., Li, B., Wen, X., Nie, X., (2021), Prestack Seismic Inversion via Nonconvex L_{1-2} Regularization. A*pplied Sciences*. 11(24): 12015. https://doi.org/10.3390/app112412015

Spitz, S., (1991), Seismic Trace Interpolation in the f-x Domain: Geophysics, 56, 785-794.

Riandy, M., (2014), Aplikasi Interpolasi F-K untuk Rekonstruksi Pseudo 3D pada Data Seismik 2D Lapangan-MR. Tugas Akhir, Jurusan Teknik Geofisika, ITB.

Trad, D., (2009), Fivedimensional interpolation: Recovering from acquisition constraints. Geophysics, Vol 74 No.6.

Triyoso, W., Irawan, J. B., Viony, N. C., Fatkhan, (2020), Application of ZO-CRS Stack on Residual PP Removal of PS Component in Converted-Wave Seismic Reflection Processing, Scientific Contributions Oil and Gas Journal, Vol. 43 No 2, 2020.

Triyoso, W., Supriyono, S., Akbar, F. S., Oktariena, M., Lestari, S., Yusuf B.E., Miraza, D., (2023), The 3D Seismic Survey Design of South Walio Offshore, Indonesia: Optimizing the 3D Survey Design Parameters, Scientific Contri- butions Oil and Gas Journal, Vol. 46 No. 2, 2023.

Xie, X., Pan, S., Luo, B., Chen, C., Chen, K., 2020, Research on Seismic Data Interpolation and Reconstruction, Journal of Physics: Conference Series, 1631(2020), 012110, IOP Publishing. doi:10.1088/1742-6596/1631/1/012110

Yang, W.Y., Wang, W., Li, G. F., (2020), Non-stationary signal inversion based on shaping regularization for random noise attenuation. Appl. Geophys. 17, 432–442.

Zhang, H., Zhang, H., Zhang, J., Hao, Y., Wang, B. (2019), An anti-aliasing POCS interpolation method for regularly undersampled seismic data using curvelet transform. Journal of Applied Geophysics, 172, 103894. https://doi.org/10.1016/j.jappgeo.2019.103894